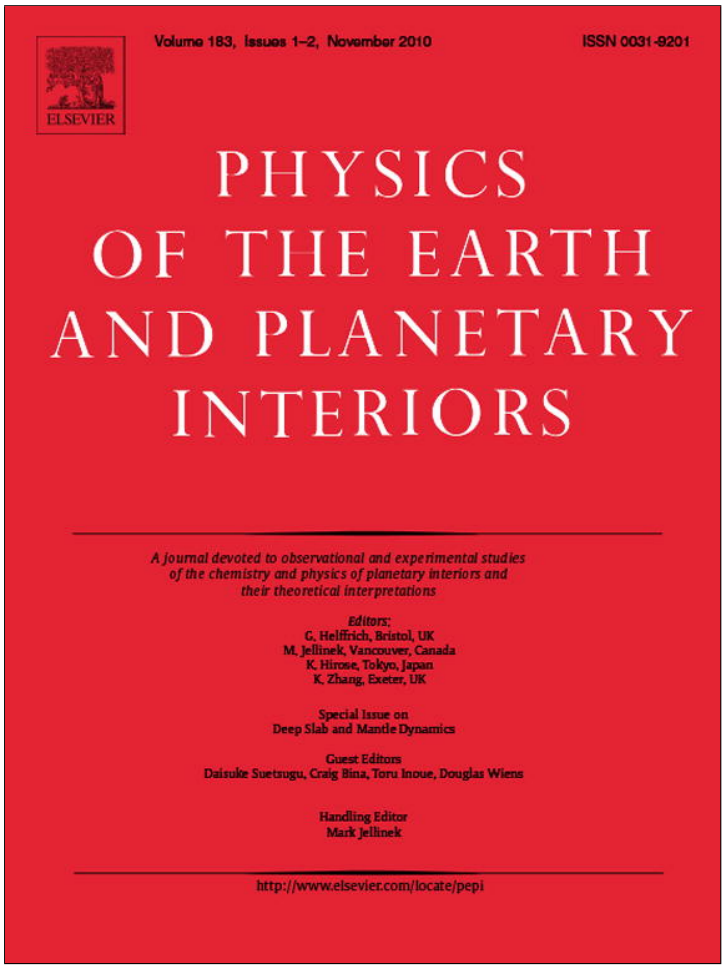

Physics of the Earth and Planetary Interiors 183 (2010) 110–114

Contents lists available at ScienceDirect

Physics of the Earth and Planetary Interiors

journal homepage: www.elsevier.com/locate/pepi

Scale limits of free-silica seismic scatterers in the lower mantle

Craig R. Bina

Department of Earth and Planetary Sciences, Northwestern University, 1850 Campus Drive, Evanston, IL 60208-2150, USA

ARTICLE INFO

Article history:
Received 10 September 2009
Received in revised form 31 March 2010
Accepted 21 June 2010

Guest Editors
Daisuke Suetsugu
Craig Bina
Toru Inoue
Douglas Wiens

Editor
Mark Jellinek

Keywords:
Diffusion
Lower mantle
Seismic scatterers
Free silica
Armored relics
Metabasalt

ABSTRACT

Lower mantle seismic scatterers are often interpreted in terms of subducted basaltic crust, which should contain free-silica phases that are seismically fast. However, free-silica phases are unstable in a peridotite lower mantle, as they react with ferropericlase (magnesiowustite) to form silicate perovskite. Nonetheless, conservative estimates and recent measurements of diffusion coefficients in silicate perovskite suggest that free-silica phases may persist as polycrystalline armored relics in lower mantle peridotite at length scales equivalent to those observed for seismic scatterers. Simple numerical simulations also suggest that polycrystalline silica may persist within subducted metabasalts.

1. Introduction

Seismic velocity anomalies and scatterers of seismic energy in the lower mantle suggest that bodies of order 100 m to 10 km in size exhibit velocity anomalies of several percent (usually fast, occasionally slow), and these often are attributed to subducted oceanic lithosphere (e.g., Kawakatsu and Niu, 1994; Niu and Kawakatsu, 1997; Hedlin et al., 1997; Kaneshima and Helffrich, 1998, 1999; Castle and Creager, 1999; Vinnik et al., 1998, 2001; Krüger et al., 2001; Niu et al., 2003; Bina 2003a; Ganguly et al., 2008; Kaneshima and Helffrich, 2009). In particular, silica-saturated basalts in oceanic crust (MORB) under lower mantle conditions should contain high-pressure phases of free silica among assemblages otherwise dominated by silicate perovskite. Estimates of modal abundances of free-silica phases in lower mantle metabasalts range from ~14% (Ricard et al., 2005; Ganguly et al., 2008) through 17–23% (Hirose et al., 2005) to larger values for more exotic compositions (Mattern et al., 2002; Bina, 2003a). Free-silica phases such as stishovite are expected to generate seismic velocity anomalies that are fast by a few percent relative to surrounding ultramafic peridotite assemblages throughout the depth range of the lower mantle (Mattern et al., 2002; Bina, 2003a; Ricard et al., 2005). Post-stishovite phases such as $CaCl_2$-structured silica may also potentially generate locally slow shear-wave velocity anomalies due to displacive shear-mode transitions (Bina, 2003b; Lakshtanov et al., 2007; Konishi et al., 2009).

All such models, however, must address the thermodynamic instability of free-silica phases in the presence of peridotites, as the silica will react with adjacent ferropericlase (magnesiowüstite) to form silicate perovskite. Thus, any free-silica phases preserved in the lower mantle may persist as armored relics, in which silica phases are insulated from surrounding ferropericlase phases by coronas of silicate perovskite (Fig. 1). This parallels the situation in crustal metamorphic rocks where, for example, staurolite crystals are often found as armored relics within garnet phases, or spinel crystals can be found as relics armored by staurolite poikiloblasts (Whitney, 1991; Gil Ibarguchi et al., 1991). In crustal metamorphic rocks, such relics generally occur at grain scales, as metamorphic fluids facilitate transport along grain boundaries. However, if lower mantle rocks are essentially dry, then larger, polycrystalline relics containing assemblages of free-silica and silicate perovskite become plausible. In such cases, the sizes of relic silica-bearing assemblages will be limited by the rate of diffusion of Si, Mg, or Fe through silicate perovskite coronas, either by volume (lattice) diffusion or by dry grain-boundary diffusion.

E-mail address: craig@earth.northwestern.edu (C.R. Bina).

0031-9201/$ – see front matter © 2010 Elsevier B.V. All rights reserved.
doi:10.1016/j.pepi.2010.06.008

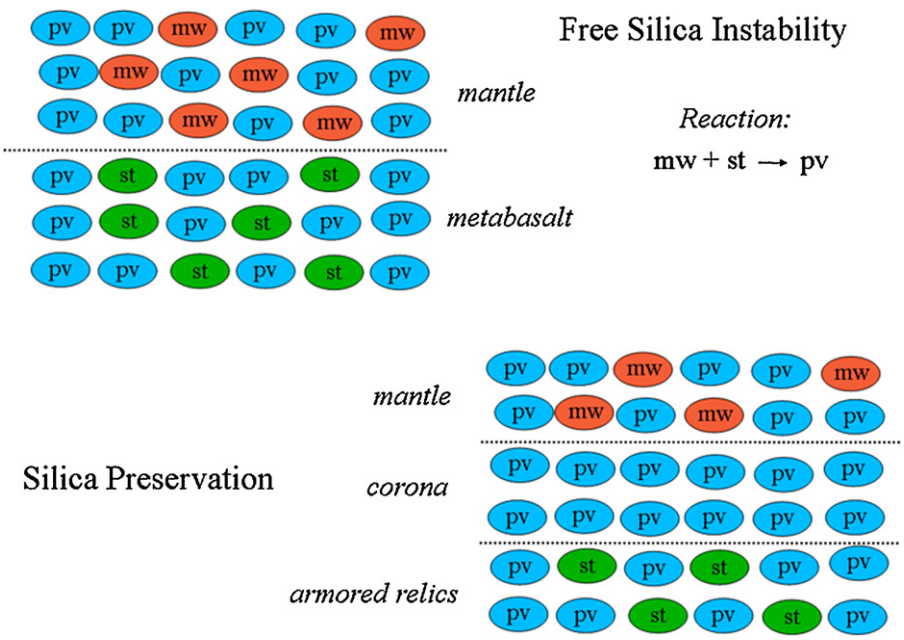

Fig. 1. Free-silica phases in lower mantle are unstable near peridotites, as silica reacts with adjacent ferropericlase (magnesiowüstite) to form silicate perovskite (top). Free-silica phases may persist as relics armored by silicate perovskite coronae at polycrystalline scale lengths in dry lower mantle (bottom).

Such formation of coronas between reactant minerals can be modeled as a combination of diffusion-controlled growth with local equilibrium (Ashworth and Sheplev, 1997). More recently, the growth of fine-grained orthoenstatite reaction rims at contacts between quartz and forsterite have been observed in the laboratory (Milke et al., 2008) and subjected to thermodynamic modeling of diffusion-controlled growth of the reaction rim (Abart et al., 2009), revealing that details of the rim growth rate may depend upon the arrangement of inclusions within the matrix. A feasibility analysis of the protection of silica relics from reaction with forsterite by armoring with orthopyroxene coronas (Ganguly and Frost, 2006) yielded a conservative estimate of the effective diffusion distance of ~10 cm over 10 Myr, for volume diffusion of Mg under dry conditions up to 10 GPa and 1623 K.

2. Diffusion rates

At a broader scale, effective diffusion coefficients of order 10^{-18} m^2/s would yield a characteristic length $L = (D \cdot t)^{1/2}$ of about 5 mm over 1 Myr. However, recent experiments suggest unusually low effective diffusion coefficients for both Si self-diffusion (Yamazaki et al., 2000) and Fe–Mg interdiffusion (Holzapfel et al., 2005) in silicate perovskite under lower mantle P, T conditions (22–26 GPa, 1973–2273 K). The resulting D values of only 10^{-20} to 10^{-18} m^2/s yield characteristic lengths of less than 5 cm over the ~60 Myr necessary for basalt subducting at ~5 cm/yr to traverse the mantle. (Here we have not treated the upper mantle separately, as analysis of silica armoring by orthopyroxene by Ganguly and Frost (2006) suggests similar length and time scales therein.) Nonetheless, rates of grain-boundary diffusion of Mg, O, and Si through pv rims may differ at the pv–st and pv–mw interfaces, and preliminary time-resolved XRD measurements (Kubo et al., 2006) of the st + mw → pv reaction (at 3–26 GPa and 1300–2000 K) show a transition from nucleation-controlled to diffusion-controlled growth, at equilibrium-boundary overstepping in excess of 1 GPa, and suggest larger D values of 10^{-16} to 10^{-15} m^2/s at 1700–1850 K. Even at these values, however, characteristic reaction lengths rise to less than 1.5 m over ~60 Myr of subduction. Thus, even for a conservative range of physically reasonable diffusion coefficients, the length scales for chemical erosion of a silica relic by diffusion through a corona of silicate perovskite remain smaller than the apparent length scales of lower mantle seismic scatterers (Fig. 2).

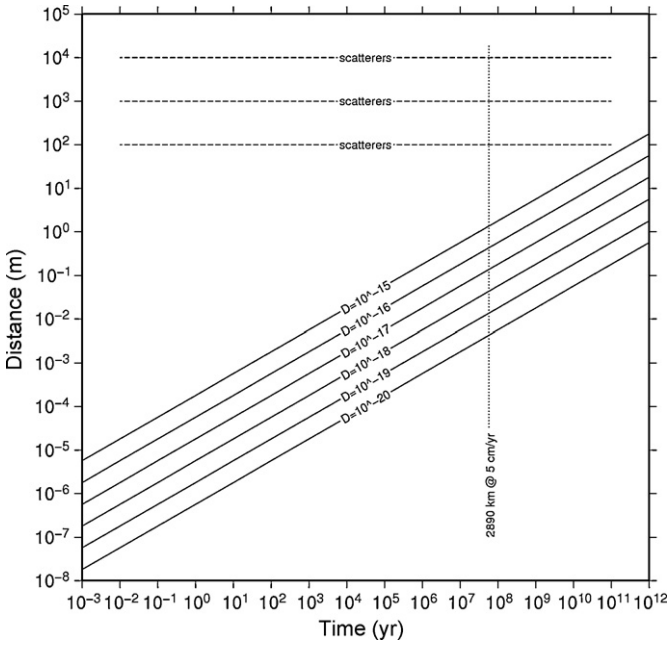

Fig. 2. Solid lines: reaction distances (i.e., length scales for penetration of corona into relic) as a function of time for various reported values of the diffusion coefficient D. Dashed lines: the range of distance scales characteristic of observed seismic scatterers in the lower mantle. Dotted line: characteristic time for basaltic crust to sink to the base of the mantle at 5 cm/yr. Note that chemical heterogeneities of the size of seismic scatterers can persist over convective time scales for all cited values of D.

3. Polycrystalline relics

Free silica will be dispersed within silica-saturated basaltic rocks such as quartz tholeiites. If subducted crust is preserved as largely intact tabular features, then reaction with surrounding peridotite

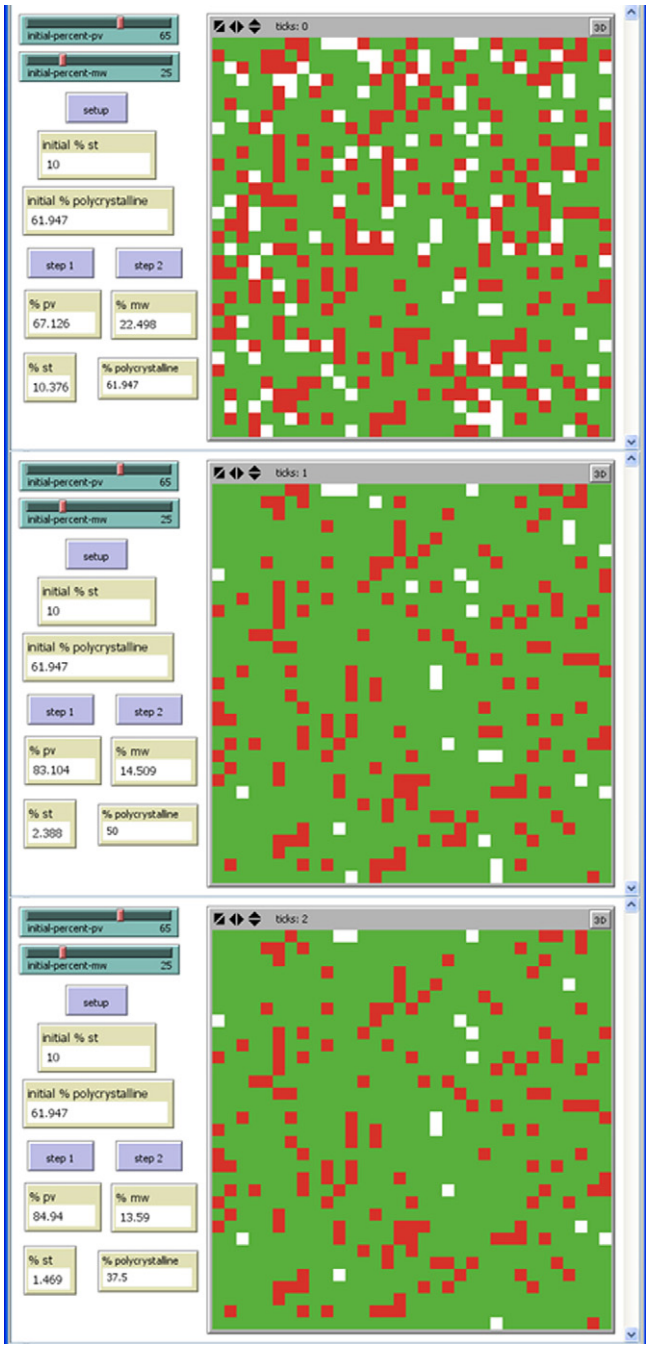

Fig. 3. An example simulation of silica preservation. Top: initial (randomly distributed) molar mineralogy for an assemblage of 65% pv, 25% mw, 10% st. Note that 62% of st phases are polycrystalline. Middle: configuration after st + mw → pv reaction between adjacent (radius = 1) phases. Note that molar mineralogy has shifted to 83% pv, 15% mw, 2% st; 50% of st phases are polycrystalline. Bottom: configuration after st + mw → pv reaction between non-adjacent (radius = 2) phases. Molar mineralogy has shifted to 85% pv, 14% mw, 1% st; 38% of st phases are polycrystalline.

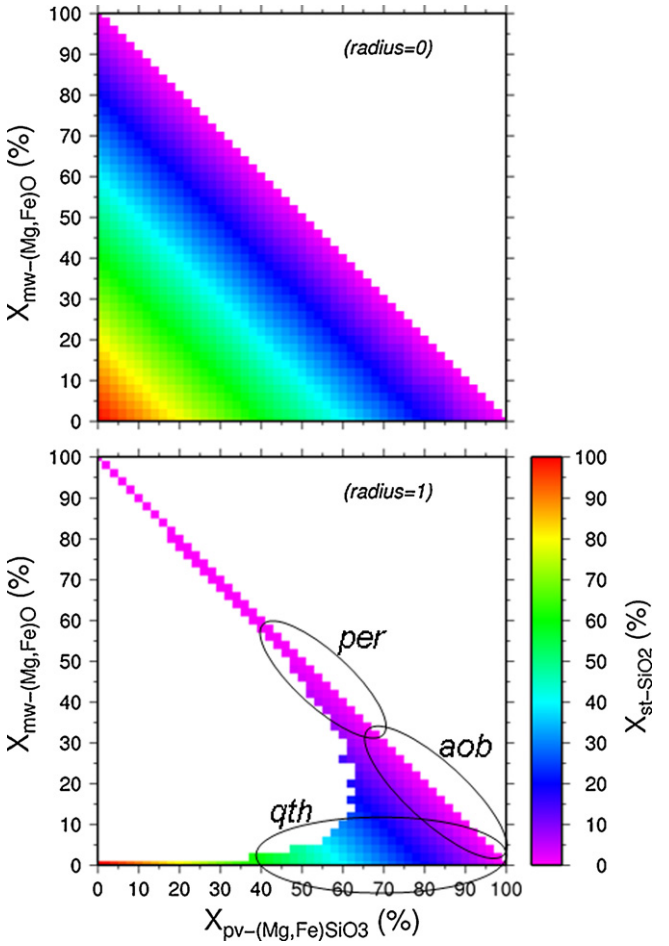

Fig. 4. Results of simulations of silica preservation, showing fraction of free silica remaining in assemblage. Top: initial conditions (radius = 0 denotes no reaction) for set of all possible phase combinations. Bottom: phase proportions after st + mw → pv reaction between adjacent (radius = 1) phases. Ellipses denote approximate loci of peridotites (per) silica-undersaturated basalts (aob), and silica-saturated basalts (*q*th).

may be confined to the margins of such features. However, in a worst case scenario for silica preservation, such metabasalts may become intimately mixed (over some characteristic length scales) with peridotite due to stretching and folding. To assess the limits of reasonable relic silica phases under lower mantle conditions, I have performed a simple simulation of the transformation of such rocks to lower mantle assemblages followed by application of the st + mw → pv reaction to adjacent phases. Using the NetLogo modeling software (Wilensky, 1999), I have parameterized model rocks (from basalts to peridotites to mechanical mixtures of the two) in terms of all possible combinations, in 1% increments, of fractions of three phases: pv-$(Mg,Fe)SiO_3$ silicate perovskite, mw-(Mg,Fe)O ferropericlase (magnesiowüstite), and st-SiO_2 stishovite. Each such rock is represented by mineral phases in the stipulated proportions, randomly distributed over a 33×33 square spatial grid (with non-wrapping boundary conditions). To these initial conditions, the st + mw → pv reaction is applied to adjacent phases (where adjacency is defined in 8 directions rather than 4). If multiple adjacent mw reactants are available to a given st phase, one is chosen at random. Simulation of a set of such randomly structured rocks, over the full space of 5101 physically realizable sets of phase proportions, is repeated ten times, and the results are averaged on each element of the 101×101 lower triangular matrix of phase proportions.

An example of this simulation for one such set of phase proportions is shown in Fig. 3. The two-dimensional image is divided into pixels, each of which represents a compositionally uniform domain of arbitrary size (not necessarily corresponding to grain scale). In the top panel, no reaction has yet occurred (i.e., the reaction radius is zero). The panel shows the initial state, with a random spatial distribution, of a pixel mineralogy for an assemblage of 65% pv, 25% mw, and 10% st. Note that 62% of st phases initially are polycrystalline (or, strictly, polypixelline). The middle panel shows the same configuration after the st + mw → pv reaction has occurred between adjacent phases (i.e., the reaction radius is one pixel). (A character-

istic time for such a radius = 1 reaction would scale with pixel size L and diffusion coefficient D as L^2/D.) After reaction, the mineralogy has shifted to 83% pv, 15% mw, and 2% st, and 50% of the st phases are polycrystalline. The bottom panel shows the same configuration after the st + mw → pv reaction has occurred between non-adjacent phases (at a reaction radius of two pixels). Molar mineralogy has shifted to 85% pv, 14% mw, and 1% st; 38% of st phases are polycrystalline. Note that pixel% values in these images are perhaps best thought of as roughly corresponding to vol.% values, as one pixel of mw reacts with one pixel of st to form two pixels (but only 1 mol) of pv. These values are converted to mol% prior to plotting in subsequent graphs.

Comparison of pre- and post-reaction conditions (Fig. 4) unsurprisingly confirms that the majority of st and mw phases are consumed by reaction (yielding pv). Little or no free silica remains in the compositional loci of peridotites (e.g., mantle lherzolites or harzburgites) or silica-undersaturated basalts (e.g., alkali olivine basalts). However, substantial fractions of free silica persist as armored relics within silica-saturated basalts (e.g., quartz tholeiites). When comparing the upper and lower panels of the figure, note, for example, that assemblages in the lower left corner of the diagram initially contain high st, low pv, and low mw. Assemblages with zero mw remain unchanged by reaction. However, assemblages with any non-zero amount of mw will be driven by reaction to higher pv and lower mw. Thus, points initially in the lower left corner migrate downward and rightward.

Furthermore, applying an additional metric to these simulations, measuring the degree of polycrystallinity of the relic silica in each rock in terms of the fraction of silica pixels which are adjacent to another silica pixel (Fig. 5), shows that significant fractions of relic silica may remain polycrystalline within the compositional locus of silica-saturated basalts. Repetition of these procedures with a diffusion radius expanded beyond adjacent phases (radius of 1) to encompass a distance of an additional pixel (radius of 2) results in small local decreases in relic silica, but the resulting graphs of aggregate behavior are essentially indistinguishable.

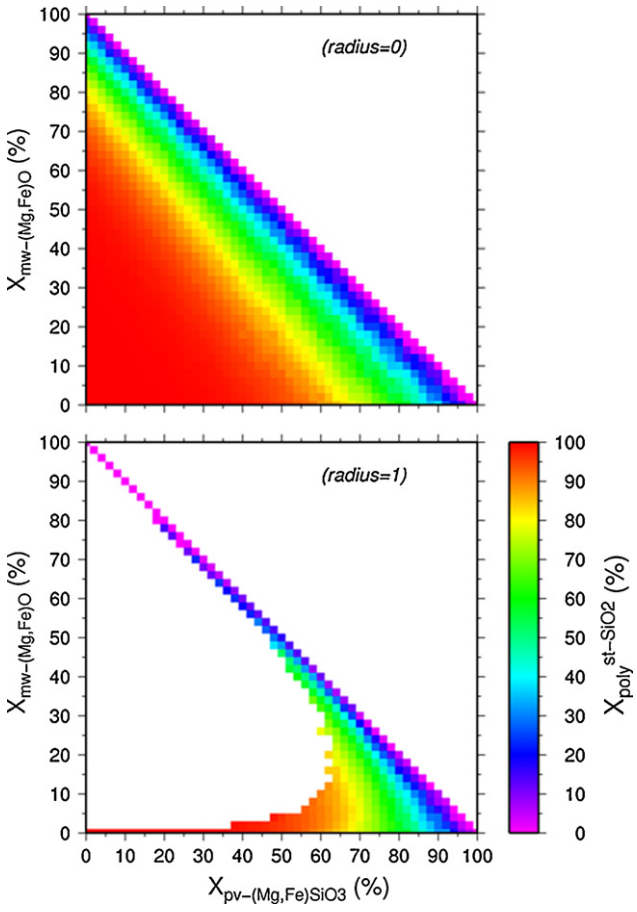

Fig. 5. Results of simulations of silica preservation, showing fraction of silica phases that remain polycrystalline. Top: initial conditions (radius = 0 denotes no reaction) for set of all possible phase combinations. Bottom: polycrystalline proportions after st + mw → pv reaction between adjacent (radius = 1) phases.

4. Concluding remarks

The preceding analyses proceed from an essentially static perpective, and the picture may be modified to some extent by dynamic effects. Subducted basaltic crust may be thinned from its initial ~10-km thickness by the effects of stretching and folding in the convecting mantle (e.g., Metcalfe et al., 1995; Van Keken et al., 2002). The effects of consequent mechanical mixing of basalt and peridotite are, however, partially addressed by the preceding numerical models. On the other hand, as diffusion scales exceed striation thicknesses during mixing, simultaneous diffusion and reaction may lead to "isolation of reactants" effects (Ottino, 1982), in which coupled diffusion and reaction may consume or disperse thinner silica-rich lamellae while preserving or enlarging (by aggregation) thicker siliceous remnants (Ottino, 1991, his Fig. 8).

However, in the absence of interconnected grain-boundary fluids or melts, polycrystalline armored silica relics potentially may persist in the lower mantle at scales of up to 0.1–10 km over time scales of order 100 Myr. Lower mantle seismic scatterers exhibit velocity anomalies of a few percent over just such length scales, of order 0.1–10 km (Hedlin et al., 1997; Cormier, 1999; Kaneshima and Helffrich, 1999; Garnero, 2000; Niu et al., 2003; Kaneshima, 2003; Cao and Romanowicz, 2007; Rost et al., 2008; Courtiers and Revenaugh, 2008; Kaneshima and Helffrich, 2009; Kaneshima, 2009).

Acknowledgements

I thank George Helffrich for helpful discussions. Figs. 2, 4, and 5 were produced using the GMT software of (Wessel and Smith, 1998). This manuscript was substantially improved based upon comments by Tomoaki Kubo and two anonymous reviewers.

References

Abart, R., Petrishcheva, E., Fischer, F.D., Svoboda, J., 2009. Thermodynamic model for diffusion controlled reaction rim growth in a binary system: application to the forsterite-enstatite-quartz system. Am. J. Sci. 309, 114–131, doi:10.2475/02.2009.02.

Ashworth, J.R., Sheplev, V.S., 1997. Diffusion modelling of metamorphic layered coronas with stability criterion and consideration of affinity. Geochim. Cosmochim. Acta 61, 3671–3689.

Bina, C.R., 2003a. Seismological constraints upon mantle composition. In: Carlson, R. (Ed.), Treatise on Geochemistry Elsevier Sci. Pub. 2, pp. 39–59.

Bina, C.R., 2003b. Seismic velocity and density anomalies from subducted basalts. In: Abstr. 8th European Workshop on Numerical Modeling of Mantle Convection and Lithospheric Dynamics, Zámek Hrubá Skála, Czech Republic, pp. 13–15.

Cao, A., Romanowicz, B., 2007. Locating scatterers in the mantle using array analysis of PKP precursors from an earthquake doublet. Earth Planet. Sci. Lett. 255, 22–31.

Castle, J.C., Creager, K.C., 1999. A steeply dipping discontinuity in the lower mantle beneath Izu-Bonin. J. Geophys. Res. 104, 7279–7292.

Cormier, C.F., 1999. Anisotropy of heterogeneity scale lengths in the lower mantle from PKIKP precursors. Geophys. J. Int. 136, 373–384.

Courtiers, A., Revenaugh, J., 2008. Slabs and shear wave reflectors in the midmantle. J. Geophys. Res. 113, B08312, doi:10.1029/2007JB005261.

Ganguly, J., Freed, A., Saxena, S., 2008. Density profiles of oceanic slabs and surrounding mantle: Integrated thermodynamic and thermal modeling, and implications for the fate of slabs at the 660 km discontinuity. Phys. Earth Planet. Int. 172, 257–267.

Ganguly, J., Frost, D.J., 2006. Stability of anhydrous phase B: experimental studies and implications for phase relations in subducting slab and the X discontinuity in the mantle. J. Geophys. Res. 111, B06203, doi:10.1029/2005JB003910.
Garnero, E.J., 2000. Heterogeneity of the lowermost mantle. Ann. Rev. Earth Planet. Sci. 28, 509–537.
Gil Ibarguchi, J.I., Mendia, M., Girardeau, J., 1991. Mg- and Cr-rich staurolite and Cr-rich kyanite in high-pressure ultrabasic rocks (Cabo Ortegal, northwestern Spain). Am. Mineral. 76, 501–511.
Hedlin, M.A.H., Shearer, P.M., Earle, P.S., 1997. Seismic evidence for small-scale heterogeneity throughout the Earth's mantle. Nature 387, 145–150.
Hirose, K., Takafuji, N., Sata, N., Ohishi, Y., 2005. Phase transition and density of subducted MORB crust in the lower mantle. Earth Planet. Sci. Lett. 237, 239–251.
Holzapfel, C., Rubie, D.C., Frost, D.J., Langenhorst, F., 2005. Fe-Mg interdiffusion in perovskite and lower mantle reequilibration. Science 309, 1707–1710.
Kaneshima, S., 2003. Small-scale heterogeneity at the top of the lower mantle around the Mariana slab. Earth Planet. Sci. Lett. 209, 85–101.
Kaneshima, S., 2009. Seismic scatterers at the shallowest lower mantle beneath subducted slabs. Earth Planet. Sci. Lett. 286, 304–315.
Kaneshima, S., Helffrich, G., 1998. Detection of lower mantle scatterers northeast of the Mariana subduction zone using short-period array data. J. Geophys. Res. 103, 4825–4838.
Kaneshima, S., Helffrich, G., 1999. Dipping lower-velocity layer in the mid-lower mantle: evidence for geochemical heterogeneity. Science 283, 1888–1891.
Kaneshima, S., Helffrich, G., 2009. Lower mantle scattering profiles and fabric below Pacific subduction zones. Earth Planet. Sci. Lett. 282, 234–239.
Kawakatsu, H., Niu, F., 1994. Seismic evidence for a 920-km discontinuity. Nature 371, 301–305.
Konishi, K., Kawai, K., Geller, R.J., Fuji, N., 2009. MORB in the lowermost mantle beneath the western Pacific: evidence from waveform inversion. Earth Planet. Sci. Lett. 278, 219–225.
Krüger, F., Baumann, M., Scherbaum, Weber, M., 2001. Mid mantle scatterers near the Mariana slab detected with a double array method. Geophys. Res. Lett. 28, 667–670.
Kubo, T., Kato, T., Nishi, M., Tominaga, A., Fukakoshi, K., 2006. Kinetics of diffusion-controlled growth of Ringwoodite and Mg-perovskite. Eos Trans. AGU 87 (Fall Meet. Suppl. (52)) (Abstr. MR21A-0005).
Lakshtanov, D.L., Sinogeikin, S.V., Litasov, K.D., Prakapenka, V.B., Hellwig, H., Wang, J., Sanches-Valle, C., Perrillat, J.-P., Chen, B., Somayazulu, M., Li, J., Ohtani, E., Bass, J.D., 2007. The post-stishovite phase transition in hydrous alumina-bearing in the lower mantle of the Earth. Proc. NAS 104, 13,588–13,590.
Mattern, E., Matas, J., Ricard, Y., 2002. Computing density and seismic velocity of subducting slabs. Eos Trans. AGU 83 (Fall Meet. Suppl. (47)) (Abstr. S51A–1011).
Metcalfe, G., Bina, C.R., Ottino, J.M., 1995. Kinematic considerations for mantle mixing. Geophys. Res. Lett. 22, 743–746.
Milke, R., Abart, R., Kunze, K., Koch-M uller, M., Schmid, D., Ulmer, P., 2008. Matrix rheology effects on reaction rim growth I: evidence from orthopyroxene rim growth experiments. J. Met. Geol. 27, 71–82, doi:10.1111/j.1525-1314.2008.00804.x.
Niu, F., Kawakatsu, H., 1997. Depth variation of the mid-mantle seismic discontinuity. Geophys. Res. Lett. 24, 429–432.
Niu, F., Kawakatsu, H., Fukao, Y., 2003. Seismic evidence for a chemical heterogeneity in the midmantle: a strong and slightly dipping seismic reflector beneath the Mariana subduction zone. J. Geophys. Res. 108 (B9), 2419.
Ottino, J.M., 1982. Description of mixing with diffusion and reaction in terms of the concept of material surfaces. J. Fluid Mech. 114, 83–103.
Ottino, J.M., 1991. Unity and diversity in mixing: stretching, diffusion, breakup, and aggregation in chaotic flows. Phys. Fluids A 3, 1417–1430.
Ricard, Y., Mattern, E., Matas, J., 2005. Synthetic tomographic images of slabs from mineral physics. In: van der Hilst, R.D., Bass, J.D., Matas, J., Trampert, J. (Eds.), Earth's Deep Interior: Structure, Composition, and Evolution, vol. 160, pp. 283–300 (Am. Geophys. Union, Geophys. Monogr.).
Rost, S., Garnero, E.J., Williams, Q., 2008. Seismic array detection of subducted oceanic crust in the lower mantle. J. Geophys. Res. 113, B06303, doi:10.1029/2007JB005263.
Van Keken, P.E., Hauri, E.H., Bellentine, C.J., 2002. Mantle mixing: the generation, preservation, and destruction of mantle heterogeneity. Annu. Rev. Earth Planet. Sci. 30, 493–525.
Vinnik, L., Kato, M., Kawakatsu, H., 2001. Search for seismic discontinuities in the lower mantle. Geophys. J. Int. 147, 41–56.
Vinnik, L., Niu, F., Kawakatsu, H., 1998. Broadband converted phases from midmantle discontinuities. Earth Planets Space 50, 987–997.
Whitney, D.L., 1991. Calcium depletion halos and Fe-Mn-Mg zoning around faceted plagioclase inclusions in garnet from a high-grade pelitic gneiss. Am. Mineral. 76, 493–500.
Wilensky, U. 1999. NetLogo. http://ccl.northwestern.edu/netlogo/. Center for Connected Learning and Computer-Based Modeling, Northwestern Univ.
Yamazaki, D., Kato, T., Yurimoto, H., Ohtani, E., Toriumi, M., 2000. Silicon self-diffusion in perovskite at 25 GPa. Phys. Earth Planet. Int. 119, 299–309.
Wessel, P., Smith, W.H.F., 1998. New, improved version of Generic Mapping Tools released. Eos Trans. Amer. Geophys. U 79 (47), 579.